University of Nebraska - Lincoln

DigitalCommons@University of Nebraska - Lincoln

1-19-2023

Antiproton collisions with excited positronium

M. Charlton

H. B. Ambalampitiya

Ilya I. Fabrikant

I. Kalinkin

D. V. Fursa

See next page for additional authors

Authors
M. Charlton, H. B. Ambalampitiya, Ilya I. Fabrikant, I. Kalinkin, D. V. Fursa, A. S. Kadyrov, and I. Bray

Antiproton collisions with excited positronium

M. Charlton ⦿

Department of Physics, Faculty of Science and Engineering, Swansea University, Swansea SA2 8PP, United Kingdom

H. B. Ambalampitiya ⦿

*Quantemol Ltd., 320 City Rd, London EC1V 2NZ, UK and Department of Physics and Astronomy, University of Nebraska,
Lincoln, Nebraska 68588-0299, USA*

I. I. Fabrikant ⦿

Department of Physics and Astronomy, University of Nebraska, Lincoln, Nebraska 68588-0299, USA

I. Kalinkin, D. V. Fursa ⦿, A. S. Kadyrov ⦿, and I. Bray ⦿

Curtin Institute for Computation and Department of Physics and Astronomy, Curtin University, GPO Box U1987, Perth WA 6845, Australia

We present results of calculations of several processes resulting from positronium (Ps) collisions with antiprotons: antihydrogen formation, Ps breakup, and n_{Ps}-changing collisions. Calculations utilize the quantum convergent close-coupling (CCC) method and the classical trajectory Monte Carlo (CTMC) method. We identify a region of Ps principal quantum numbers n_{Ps} and Ps energies where the classical description is valid and where the CCC calculations become computationally too expensive. This allows us to present the most complete and reliable set of cross sections in a broad range of n_{Ps} and initial orbital momentum quantum numbers l_{Ps} which are necessary for experiments with antihydrogen at CERN.

I. INTRODUCTION

For the last decade or so it has become possible to trap and accumulate atoms of antihydrogen ($\overline{H}$), the antiproton-positron ($\overline{p}$-e^+) bound state (see, e.g., Refs. [1–3]). This has facilitated studies of some of the properties of the antiatom, notably, measurement of the ground-state hyperfine splitting [4], determination of the two-photon 1*s*-2*s* transition at a level of a few parts in 10^{12} [5], and observation of the 1*s*-2*p* Lyman-α line [6] and its use to demonstrate laser cooling of a trapped sample of the anti-atoms [7]. The motivation for undertaking these difficult experiments has been expounded on at length elsewhere [8], and includes tests of symmetry as searches for departures from the standard model of particle physics, and antimatter tests of the weak equivalence principle of general relativity.

With respect to the latter, three experiments located at CERN's "Antimatter Factory" [9,10] intend to study the gravitational behavior of $\overline{H}$. The ALPHA Collaboration plans to analyze the trajectories of antiatoms on escape from a vertical trapping apparatus [11], while both AEgIS [12] and GBAR [13] aim to use (albeit in quite different ways) excited states of positronium (Ps, the e^+-e^- bound state) to create $\overline{H}$, as an intermediary in their respective experimental approaches, via the reaction

$$\text{Ps}(n_{Ps}, l_{Ps}) + \overline{p} \rightarrow \overline{H}(n_{\overline{H}}, l_{\overline{H}}) + e^-. \quad (1)$$
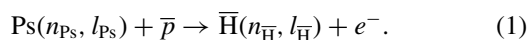
AEgIS plan to use Stark acceleration of Rydberg $\overline{H}$ to create an antiatom beam for an interferometry approach to measur-

ing antimatter gravitation, while GBAR intend to use a further charge-exchange reaction involving Ps to form the antihydrogen anion, $\overline{H}^+$, which will be captured and cooled in an ion trap before the excess positron is removed by photoionization to leave the remnant $\overline{H}$ free to fall in the Earth's gravitational field. These experiments have been made possible by the development of the ELENA facility [10] at CERN, which has enhanced the yield of trapped antiprotons for antimatter experiments, as well as the capability to routinely produce clouds of excited Ps atoms in the laboratory; see Ref. [14] for an authoritative review of the latter.

For GBAR and AEgIS, the (respective) yields of $\overline{H}^+$ and $\overline{H}$ are low, and it is prudent to estimate reaction rates and probabilities using the most accurate cross section data available for reaction (1). Experimental observations of this reaction [15] and its charge conjugate involving proton impact [16] are sparse, such that we are almost completely reliant upon accurate theory to support fundamental experimental development and to assess the feasibility of proposed reaction schemes. Thus, there is an urgent need for detailed, benchmarked theoretical data over as wide a range of initial Ps states as possible, and in the low (sub-eV) kinetic-energy range of most interest to experiment.

In response to these experimental requirements, we present the results of calculations involving quantum convergent close-coupling (CCC) [17]) and classical trajectory Monte Carlo (CTMC) [18,19] techniques. Our work builds upon, and enhances, our previous studies [19–24] for reaction (1) as well as for Ps breakup and collisions involving Ps state-change,

reactions (2) and (3), respectively, as

$$\text{Ps}(n_{\text{Ps}}, l_{\text{Ps}}) + \overline{p} \rightarrow \overline{p} + e^+ + e^- \quad (2)$$

and

$$\text{Ps}(n_{\text{Ps}}, l_{\text{Ps}}) + \overline{p} \rightarrow \text{Ps}(n'_{\text{Ps}}, l'_{\text{Ps}}) + \overline{p}. \quad (3)$$

We note that though our focus here is on $\overline{\text{H}}$ formation, our data have implications for Ps-ion reactions in general, which have been suggested as a possible source of cold atoms [25].

The remainder of the article is organized as follows. Section II contains a brief description of the CCC and CTMC methodologies, with the results for reactions (1)–(3) presented in Sec. III, along with a discussion of their relevance for experiment.

II. THEORY

A. Convergent close coupling

The details of the CCC theory for application to the two-center problem of e^+-H scattering have been given by Kadyrov and Bray [17], with a wide range of applications reviewed more recently [26]. Due to time-reversal invariance, this is equivalent to $\text{Ps} - p$ scattering, which in turn is equivalent to the $\text{Ps} - \overline{p}$ collision system, which has $\overline{\text{H}}$ formation as one of the channels. Briefly, the total wave function is expanded utilizing states obtained in both the H and Ps centers, by diagonalizing the corresponding Hamiltonians in the Laguerre basis

$$\xi_{kl}(r) = \sqrt{\frac{\lambda_l(k-1)!}{(2l+1+k)!}} (\lambda_l r)^{l+1} \exp(-\lambda_l r/2) L_{k-1}^{2l+2}(\lambda_l r), \quad (4)$$

where $L_{k-1}^{2l+2}(\lambda_l r)$ are the associated Laguerre polynomials, and k ranges from 1 to the basis size N_l.

Upon the expansion, the close-coupling equations are formed and solved in momentum space. The CCC calculations depend on several parameters of the Laguerre basis for their convergence. These are the maximum orbital angular momentum of the expansion states $l_{\max}$, the number of Laguerre basis functions N_l, and the corresponding exponential fall-offs λ_l. These are independent for both centers of the problem. In the presentation by Charlton *et al.* [24] the CCC calculations had $l_{\max}^{\text{Ps}} = 6$ and $l_{\max}^{\text{H}} = 8$, $\lambda_l^{\text{Ps}} = 0.25$ and $\lambda_l^{\text{H}} = 0.5$, and $N_l = 30 - l$ for both the H and Ps states. Such calculations may be denoted as $\text{CCC}(30_8, 30_6)$. It was noted that while most of the presented transitions were indeed convergent, the breakup cross sections for $\text{Ps}(n_{\text{Ps}}, l_{\text{Ps}})$, for the larger values of n_{Ps} were not. Following extensive computer code optimization, here we present the results of $\text{CCC}(30_9, 30_9)$ calculations, i.e., the $l_{\max} = 9$ for both centers. In that context the present CCC results supersede those of Charlton *et al.* [24]. Furthermore, the earlier presented results were aggregated over the initial and final states, whereas here we present far more detail.

The energy levels in the $\text{CCC}(30_9, 30_9)$ calculations are given in Fig. 1. The negative-energy states correspond to bound atomic and Ps states. The positive-energy states correspond to the atomic and Ps continuum. As the expansion states on the two centers are not orthogonal, it may appear that there is double-counting of the continuum. This issue
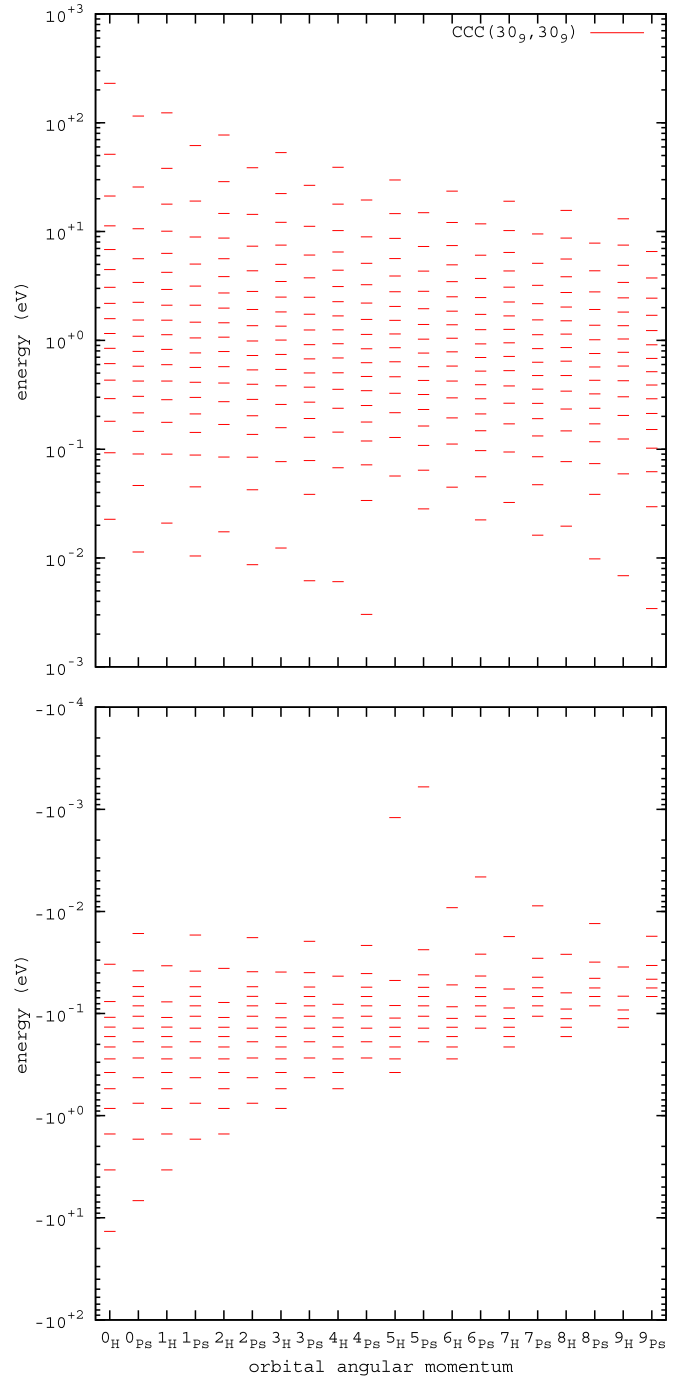

FIG. 1. Energies of the H and Ps states used in the $\text{CCC}(30_9, 30_9)$ calculations, where the number of Laguerre-based states on both the H and Ps centers is $30 - l$ for $0 \leqslant l \leqslant 9$, for a total of 255 states for each center.

has been studied extensively [27,28]. The essential conclusion is that there is no formal double-counting due to cross sections being defined at infinite separations of the two centers, with both sets of the expansion states having exponential fall-offs λ_l, see Eq. (4). However, the rate of convergence and the ill-conditioning of the close-coupling equations can be substantially affected by the way the continuum is treated. This is particularly an issue presently as such large expansions

have not been previously undertaken for the collision problem of interest.

B. CTMC

The theory of CTMC for a three-body system consisting of charged particles where two of them are bound is described in Refs. [29,30]. The CTMC approach has been applied before in the case of a Ps atom interacting with a proton [18,19,24,31], and recently extended to the laser-assisted case [32]. The theory is described in brief as follows. For a given impact parameter and the principal quantum number n_{Ps} of the projectile Ps atom, an ensemble of initial states is prepared by a random selection of the eccentricity, the orientation of the mutual motion (Kepler orbits) of the $e^- - e^+$ pair, and the position of e^- on the orbit. A classical trajectory for each random state is then propagated towards the proton which is stationary at the origin of the configuration space.

The Hamiltonian equations are solved using the regularization method described in Refs. [33,34]. The solutions are propagated giving sufficient time for the interaction with the target. At the end of the propagation, the final energies and the angular momenta of the trajectories are checked to generate the statistics in different final channels to calculate the probabilities and cross sections. For example, the charge-transfer probability $P(b)$ as a function of the impact parameter b is computed as a ratio between the number of trajectories leading to the formation of the final atom and the total number of sampled trajectories. The charge-transfer cross section σ_{CT} is then given by the integral $\int 2\pi P(b) b \, db$. The total number of trajectories for each energy point was varied between 6×10^4 and 10^6 to make sure that the statistical error for the cross section is less than 1%.

III. RESULTS AND DISCUSSION

Cross sections for $\overline{H}$ formation and Ps breakup [reactions (1) and (2)], disaggregated by Ps state up to $n_{Ps} = 7$ and $l_{Ps} = 6$, and with appropriately [see Eq. (6)] scaled magnitude and Ps kinetic energy scales, are shown in Figs. 2–8 for both the CCC and CTMC approaches.

We note a few general features: first, at low Ps kinetic energies and for $n_{Ps} \leqslant 2$ the CTMC $\overline{H}$ formation results are very different from the CCC data, which are certainly the more accurate of the two. (Recall that the CCC data for $n_{Ps} = 1$ have previously been validated [20,21] against the very accurate variational work of Humberston and co-workers [35].) For $n_{Ps} > 2$, and independent of the Ps angular momentum, there is good accord between the CCC and CTMC data for reaction (1) across the Ps kinetic energy range, except at the highest energies (where the cross sections are falling rapidly), where the CTMC data seem to fall faster than those for CCC. The behavior of the exothermic $\overline{H}$ formation reaction at low energies has been discussed elsewhere [20,21] and the data show little dependence on l_{Ps}, certainly for $n_{Ps} > 2$.

Turning next to reaction (2), breakup, it is notable that there are significant differences near the threshold [which occurs at the scaled Ps kinetic energy of 6.8 eV = 0.25 atomic units (a.u.)] between the CCC and CTMC results, with the latter

FIG. 2. Integrated cross sections of total $\overline{H}$ formation and breakup for $Ps(n_{Ps}, l_{Ps}) - \bar{p}$ scattering for $l_{Ps} = 0$.

falling markedly below the former. This effect appears to increase with the higher values of n_{Ps}. At the higher kinetic energies, and above the maximum in the cross section which occurs at the scaled energy of around 1 a.u., the two calculations are in excellent accord. We note that the results for reactions (1) and (2) cross just below the maximum in the latter in all cases, and in this energy range the $\overline{H}$ formation cross section is falling rapidly and becomes negligible by a scaled kinetic energy of $10/n_{Ps}^2$ a.u.
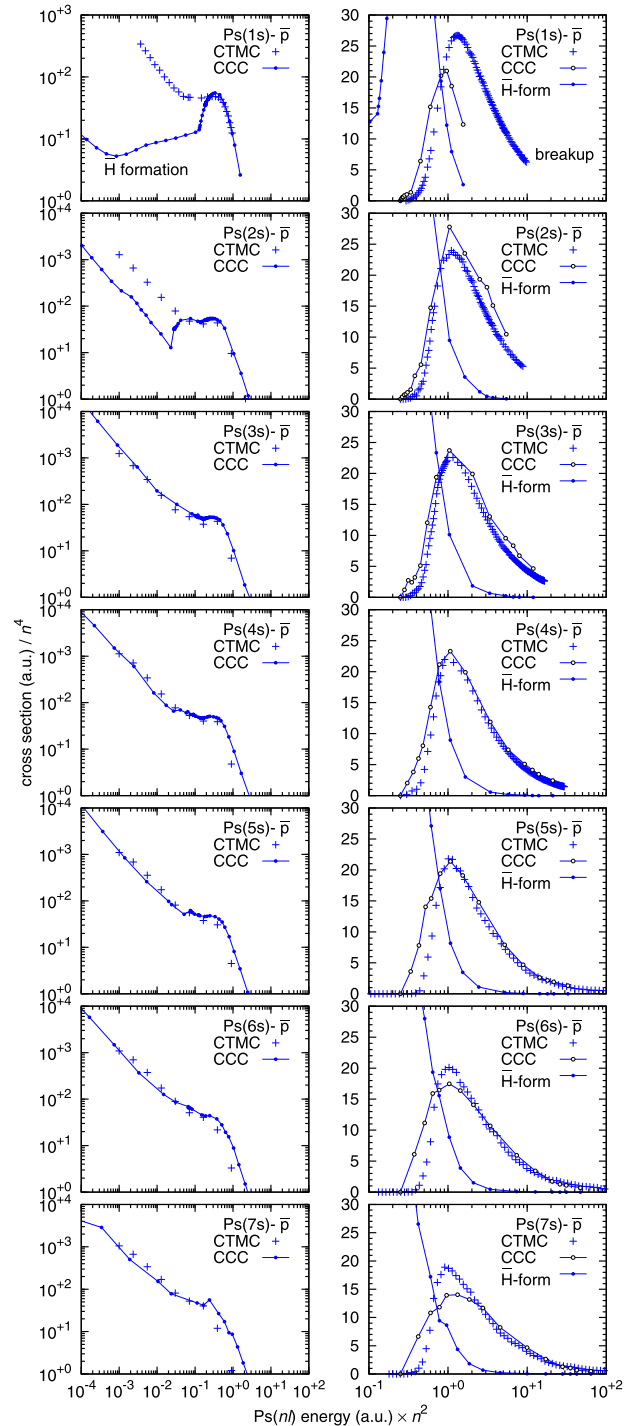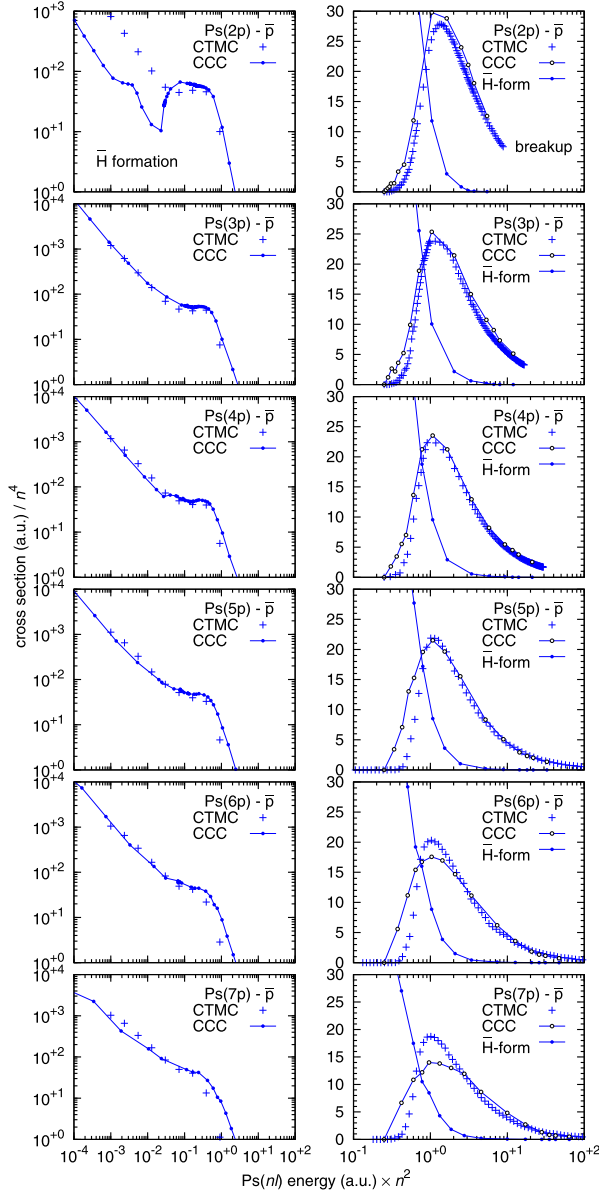
FIG. 3. Integrated cross sections of total $\bar{\text{H}}$ formation and breakup for $\text{Ps}(n_{\text{Ps}}, l_{\text{Ps}}) - \bar{p}$ scattering for $l_{\text{Ps}} = 1$.

Investigations have found that the classical Ps(1s) breakup cross section can be fit in the near-threshold region by the Wannier law [36] with Klar's [37] exponent $\mu = 2.65$,

$$\sigma_1(E) = CE^\mu, \quad (5)$$

where $E \geqslant 0$ is the total energy, and the coefficient C depends on the choice of energy units. For the energy unit of electron volts, using the CTMC cross sections we find $C = 0.020$ to yield the cross section in atomic units. If energy is measured in atomic units, then $C = 126.8$. Although the Klar derivation was carried out for positron-impact ionization of H, it was based on the analysis of the quasiclassical wave function of the final-state three-body system, therefore, it is equally applicable to the Ps breakup process.

According to the classical scaling laws [29,38,39], the cross section for a process involving a hydrogen-like system in the initial state (nl) and relative collision energy ϵ can be
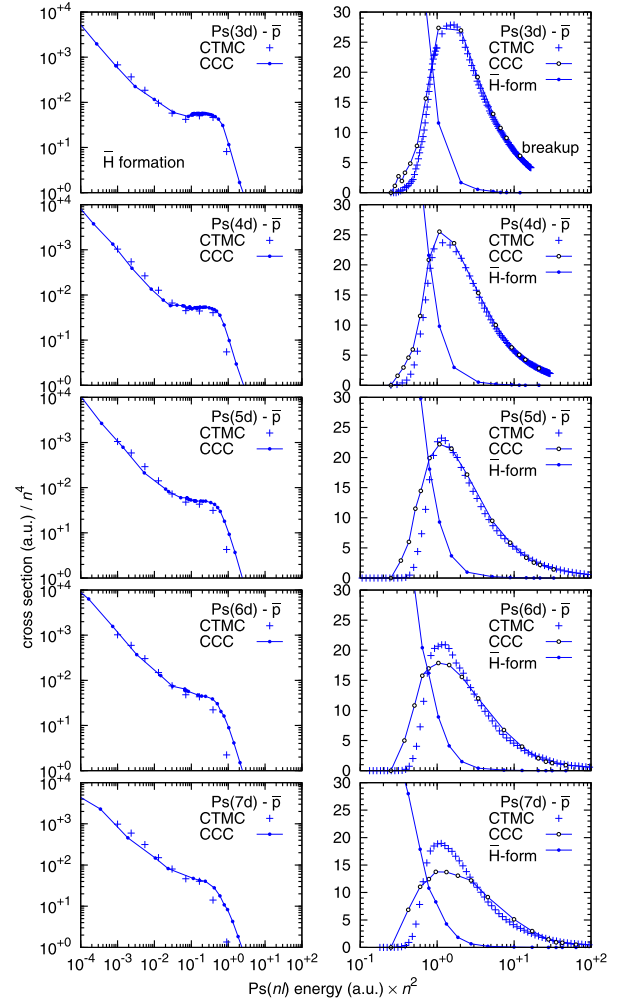

FIG. 4. Integrated cross sections of total $\bar{\text{H}}$ formation and breakup for $\text{Ps}(n_{\text{Ps}}, l_{\text{Ps}}) - \bar{p}$ scattering for $l_{\text{Ps}} = 2$.

calculated as

$$\sigma_{nl}(E) = n^4 \sigma_{1,l/n}(n^2\epsilon), \quad (6)$$

where principal quantum number n and orbital angular momentum quantum number l are treated as continuum variables. For the cross section averaged over initial angular momentum states we obtain

$$\sigma_n = \frac{1}{n^2} \sum_l (2l+1)\sigma_{nl}(\epsilon) = n^2 \sum_l (2l+1)\sigma_{1,l/n}(n^2\epsilon),$$

which can be approximately written as

$$\sigma_n = n^4 \sigma_1(n^2\epsilon) \quad (7)$$

for some average value of l/n between 0 and 1. Since l/n is related to the eccentricity of the orbit, this averaging occurs naturally in CTMC calculations for $n = 1$ when initial conditions are chosen from the microcanonical distribution.

Apply now the classical scaling to the Wannier law, Eq. (5), where $E = \epsilon - \epsilon_t$. For the Ps($n=1$) breakup process $\epsilon_t = 0.25$ a.u. For an arbitrary $n = n_{\text{Ps}}$ we obtain

$$\sigma_n = Cn^{4+2\mu}E^\mu, \quad (8)$$
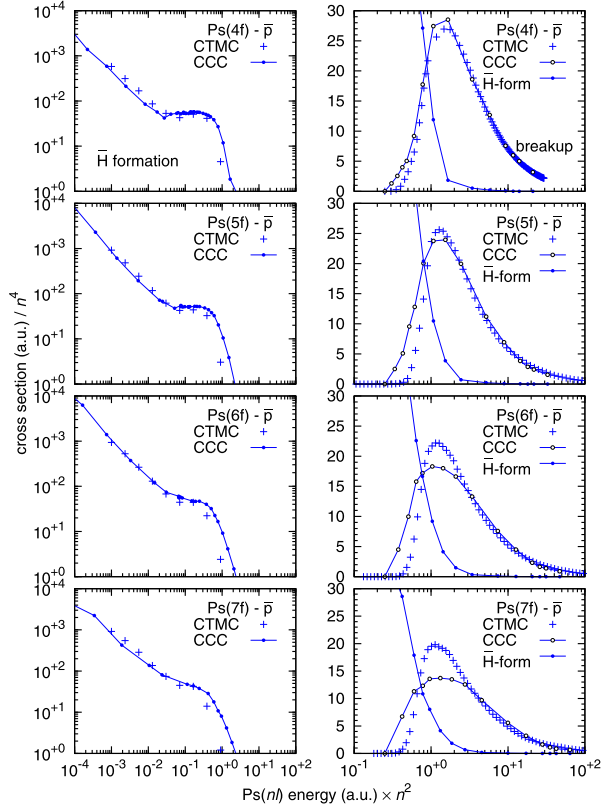
where $E = \epsilon - \frac{\epsilon_t}{n^2}$.

FIG. 5. Integrated cross sections of total $\bar{\text{H}}$ formation and breakup for $\text{Ps}(n_{\text{Ps}}, l_{\text{Ps}}) - \bar{p}$ scattering for $l_{\text{Ps}} = 3$.

The computed l-averaged cross sections can be fit with a high precision by Eqs. (5) and (8). For l-specific cross sections the proportionality constant depends on l, and a more sophisticated parametrization [39] can be introduced for these. Though for breakup the Wannier threshold law has been
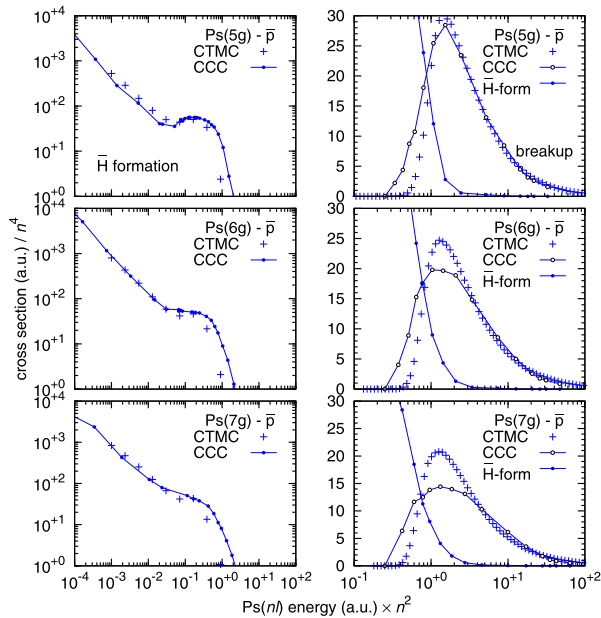

FIG. 6. Integrated cross sections of total $\bar{\text{H}}$ formation and breakup for $\text{Ps}(n_{\text{Ps}}, l_{\text{Ps}}) - \bar{p}$ scattering for $l_{\text{Ps}} = 4$.
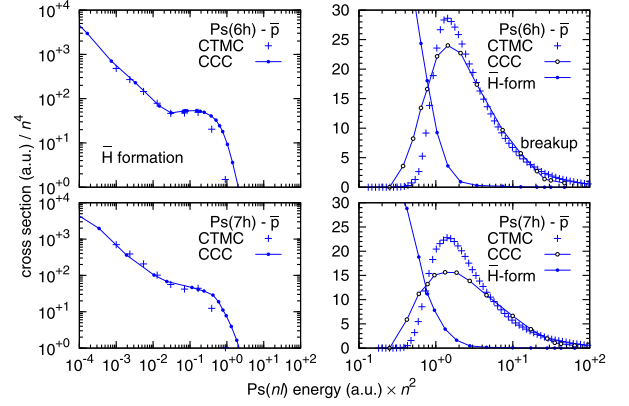

FIG. 7. Integrated cross sections of total $\bar{\text{H}}$ formation and breakup for $\text{Ps}(n_{\text{Ps}}, l_{\text{Ps}}) - \bar{p}$ scattering for $l_{\text{Ps}} = 5$.

confirmed over a small energy range by most quantum calculations, including CCC [40], it is apparent that the CCC and CTMC cross section behavior is rather different, particularly with increasing n_{Ps}. Unfortunately, the size of the CCC calculations prohibits a very detailed examination of this region. However, what is particularly important from the experimental perspective is the region where there is the transition from $\bar{\text{H}}$ formation dominance to the breakup dominance. This is shown on the right-hand-side panels of Figs. 2–8, where we see good agreement between the CCC and CTMC cross sections.

The transition between the dominance of $\bar{\text{H}}$ formation and Ps breakup occurs at a Ps kinetic energy of around $1/n_{\text{Ps}}^2$ a.u., or if the antiatom is to be formed in a beam directly via reaction (1), an equivalent antiproton kinetic energy in the kiloelectron volt region. In particular, this may have implications for the experimental scenario of the GBAR collaboration, which will use a kiloelectron volt antiproton beam to cross a cloud of Ps atoms to produce the antiatoms.

The CCC data for $\bar{\text{H}}$ formation are shown in more detail in Figs. 9–14, with the final antiatom state explicit for the initial Ps ground state and the first few excited states up to and including $n_{\text{Ps}} = 3$. The behavior is complex and changes as the Ps principal quantum number increases. The threshold, E_{th}, for $\bar{\text{H}}$ formation is given by

$$E_{\text{th}} = \frac{1}{2}\left(\frac{1}{2n_{\text{Ps}}^2} - \frac{1}{n_{\bar{\text{H}}}^2}\right) \text{a.u.}, \qquad (9)$$

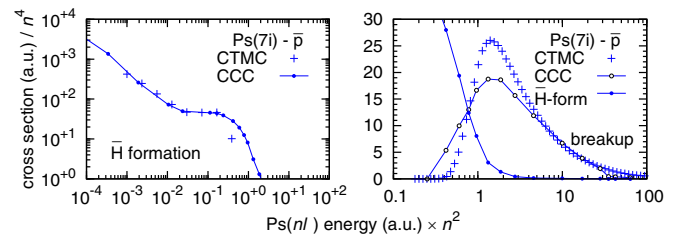such that the reaction is exothermic when $\sqrt{2}n_{\text{Ps}} > n_{\bar{\text{H}}}$.

FIG. 8. Integrated cross sections of total $\bar{\text{H}}$ formation and breakup for $\text{Ps}(n_{\text{Ps}}, l_{\text{Ps}}) - \bar{p}$ scattering for $l_{\text{Ps}} = 6$.
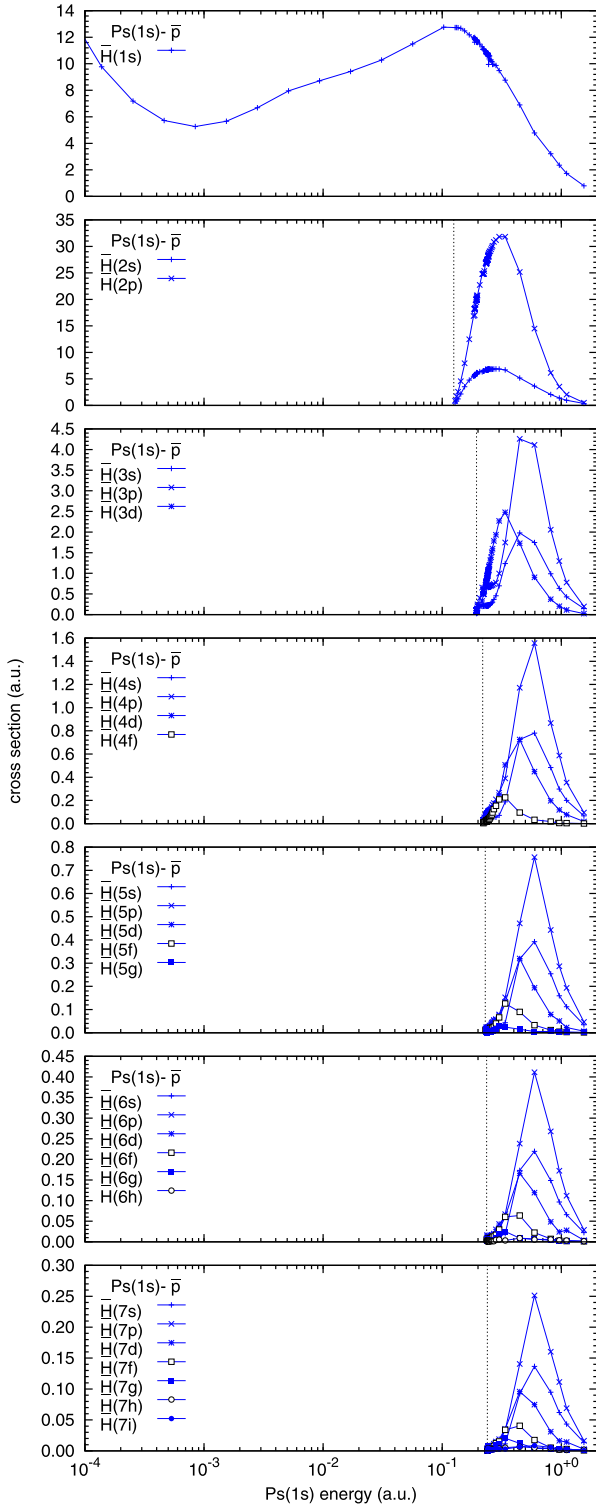
FIG. 9. CCC-calculated integrated cross sections of $\bar{\mathrm{H}}$ formation in specified states for Ps(1s) $-\bar{p}$ scattering. The vertical dotted line indicates the excitation threshold.

FIG. 10. As for Fig. 9, except for Ps(2s) $-\bar{p}$ scattering.

At the lowest kinetic energies the exothermic reactions dominate, with the most likely states being those closest to the energy resonance condition, $n_{\bar{\mathrm{H}}} = \sqrt{2} n_{\mathrm{Ps}}$, as pointed out in this context some time ago [41]. For these reactions all $\bar{\mathrm{H}}$ angular momentum states contribute, and with increasing
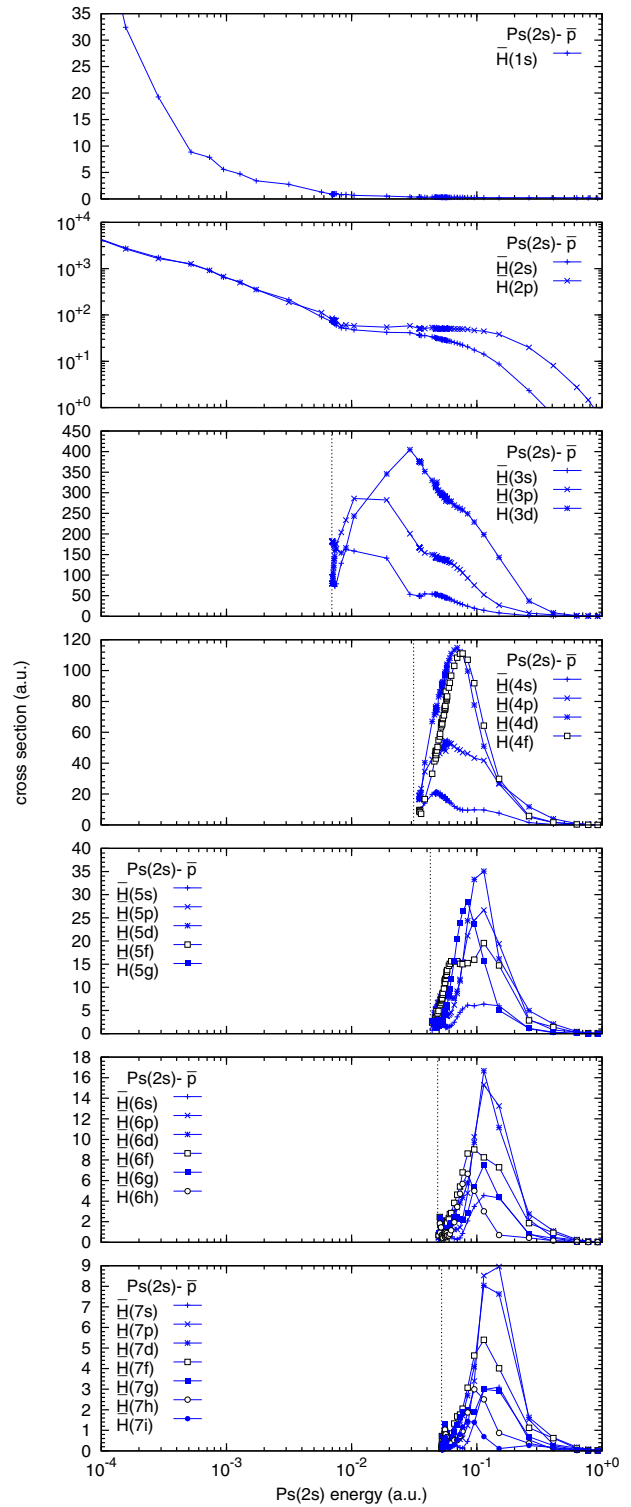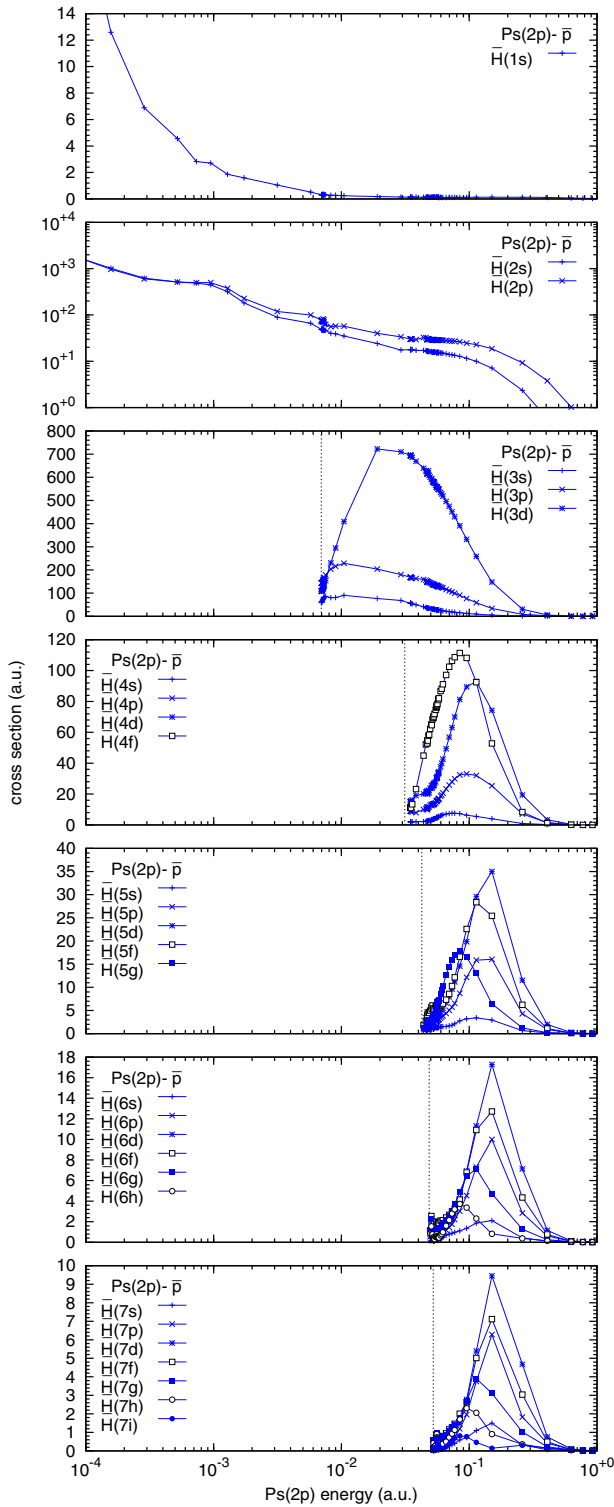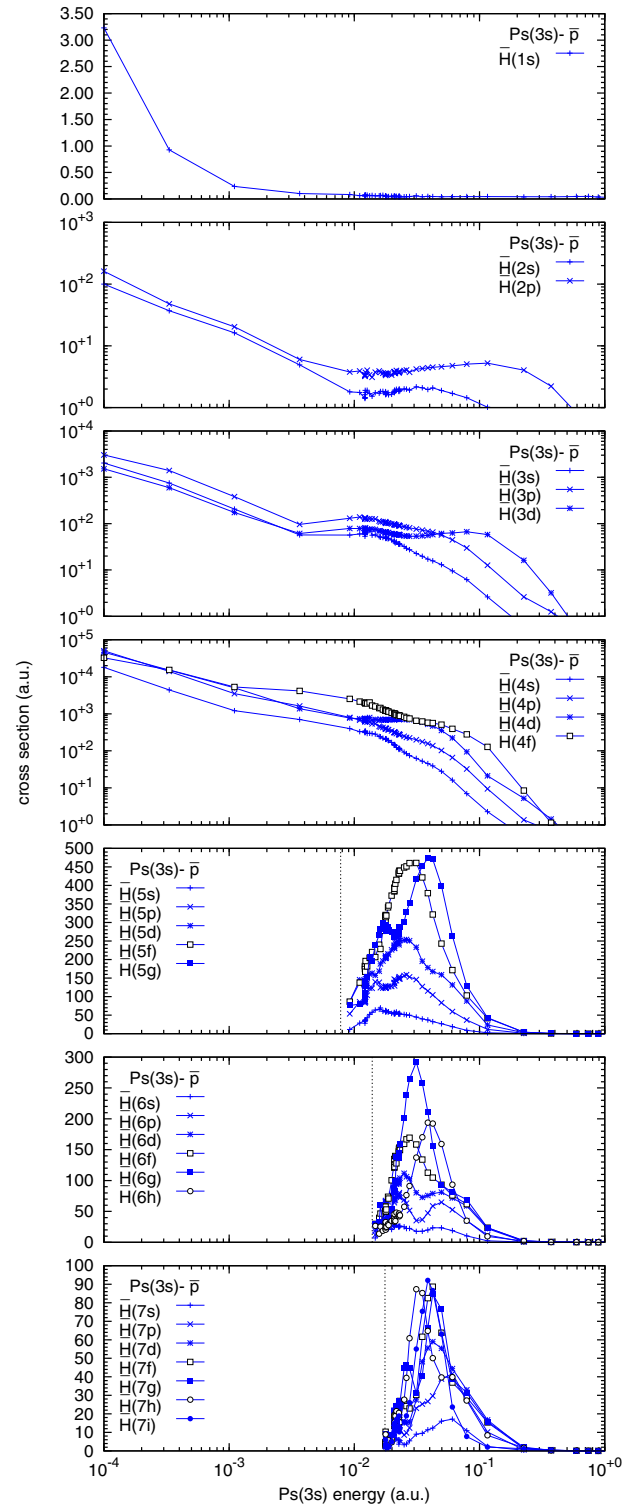
values of $(n_{\mathrm{Ps}}, l_{\mathrm{Ps}})$, it is found that higher values of $l_{\bar{\mathrm{H}}}$ are the most important, particularly in the dominant $n_{\bar{\mathrm{H}}}$ manifold.

The behavior of the cross sections for the endothermic states of reaction (1) again shows that all $\bar{\mathrm{H}}$ angular momentum states are populated, and they can make a significant contribution to the overall $\bar{\mathrm{H}}$ yield in the Ps kinetic-energy

FIG. 11. As for Fig. 9, except for Ps(2p) − p̄ scattering.

FIG. 12. As for Fig. 9, except for Ps(3s) − p̄ scattering.

range over which they are important (from 10^{-1}-1 a.u. for $n_{Ps} \leqslant 2$ and for 10^{-2}-10^{-1} a.u. for $n_{Ps} = 3$). In general, the cross sections rise sharply from threshold to a peak, before falling to close to zero by a Ps kinetic energy of around 1 a.u.

We now consider the Ps ground (1s) state and the $n_{Ps} = 2$ and 3 states in more detail, given that the Ps is typically produced in the 1s state following positron impact onto a prepared target, and since most of the lower excited states can be readily reached from the ground state (see, e.g., Refs. [42–45]). These states are also those of most relevance for the GBAR experiment for the promotion of $\overline{H}^+$ formation, for which the antiatom should be in the ground state, though the Ps can be in its ground state, or a low excited state [46–49].
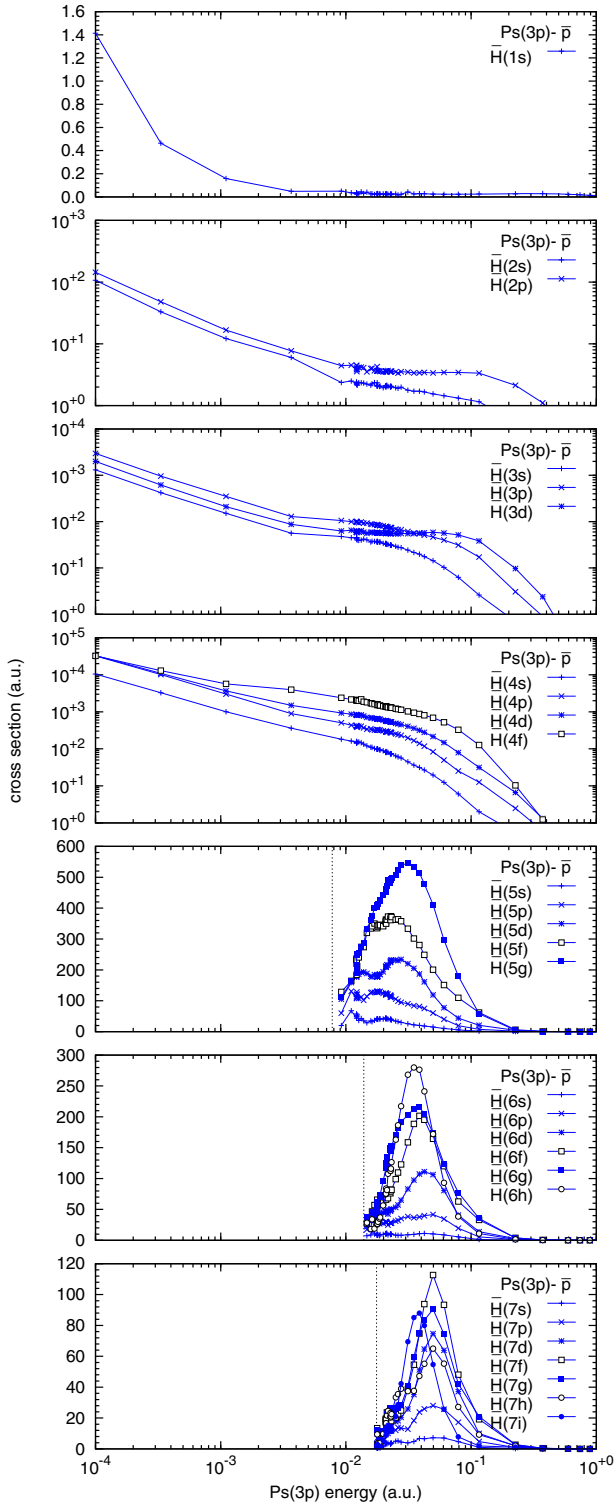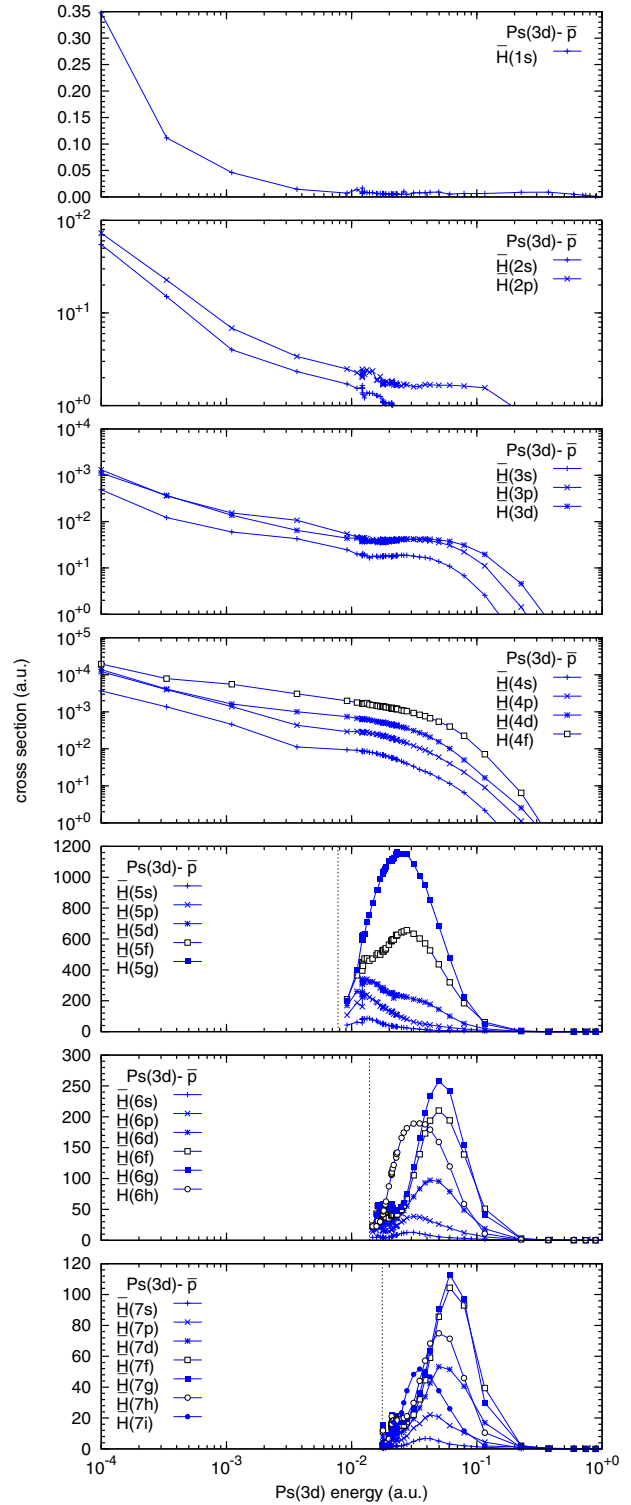
FIG. 13. As for Fig. 9, except for Ps(3p) − p̄ scattering.

FIG. 14. As for Fig. 9, except for Ps(3d) − p̄ scattering.

For the $1s$ state shown in Fig. 9 only formation of $\overline{\text{H}}(1s)$ is exothermic, and it is the only channel available below formation into the $n_{\overline{\text{H}}} = 2$ states, which open [from Eq. (9)] at a Ps kinetic energy threshold of 0.125 a.u. At low energies the cross section behaves as $E^{-1/2}$, according to the Bethe-Wigner threshold law. The data for the endothermic reactions (i.e., formation into excited states up to $n_{\overline{\text{H}}} = 7$)

share a number of features: (i) the cross section is finite at the threshold, according to the Gailitis-Damburg threshold law [50,51], and typically rises sharply, peaking after a few electron volts; (ii) in all cases, formation into the p states dominates, with significant contributions also from the s- and d- (where applicable) states, and (iii) for the higher values of $n_{\overline{\text{H}}}$, the contribution from the higher angular momentum states

is small. It is notable that formation into the $n_{\overline{H}} = 2$ manifold has the highest cross section, and indeed, at its maximum, the $2p$-state yield exceeds the sum of all the other possible states combined.

Data for the $n_{Ps} = 2$ states are shown in Figs. 10 and 11, where it is clear that antiatom formation into the $n_{\overline{H}} = 2$ states is now an exothermic process. Note that low-energy behavior of the exothermic process is now different: the cross section behaves as $1/E$ [50,51]. Below the $n_{\overline{H}} = 3$ threshold at 0.00694 a.u., formation into the $n_{\overline{H}} = 2$ states dominates, with cross sections for the Ps($2s$) target roughly three times those for Ps($2p$) at equal Ps kinetic energies, and with the final antiatom s- and p states contributing roughly equally.

Once the endothermic channels open, they quickly dominate the $\overline{H}$ yield with, as expected, formation into the $n_{\overline{H}} = 3$ states having the largest cross sections; and now the contribution from the Ps($2p$) states are greater than those from $2s$. In general, cross sections for formation into the $\overline{H}$ d state are larger than those for other angular momenta across the raft of antiatom principal quantum numbers. The $\overline{H}$ s state typically has a minor role, and there are important contributions from higher angular momenta, but overall, the dominant yield is due to the $(3d + 3p)$ combination, for both Ps states.

The results for $n_{Ps} = 3$ are given in Figs. 12–14. All antiatom states, with $n_{\overline{H}} \leqslant 4$ are exothermic with $n_{\overline{H}} = 4$ having the highest cross section for all Ps states. For these reactions, formation into the p state of the antiatom is dominant in most cases, but there are significant contributions from all $l_{\overline{H}}$ states. As expected from earlier work [24], the magnitude of the cross section is much increased over those for $n_{Ps} = 2$. Although the results fall dramatically with increased Ps kinetic energy, they are large enough to be significant when the endothermic reactions open at 0.007 a.u., in marked contrast to the situation for the $n_{Ps} = 1, 2$ states.

The cross sections for the endothermic reactions display peaked structures that are similar to those found for the lower Ps states, but with much larger contributions from the higher antiatom angular momentum states.

Finally, data for Ps state-changing ($n_{Ps} \rightarrow n'_{Ps}$) collisions [reaction (3)] of relevance to the GBAR effort are shown in Figs. 15–20. Overall, the cross sections display complex dependencies on the final $\overline{H}$ state, but are generally smaller than, or comparable to, those for antiatom formation. As a result, they should have only a minor effect on the overall $\overline{H}$ formation, and in the case of GBAR, $\overline{H}^+$ yields.

We should note, though, that l-mixing collisions without change of the n_{Ps} quantum number have much higher cross sections, which were investigated in Refs. [52,53]. In the region between 0.003 and 1 eV elastic cross sections behave as A/E, where A is a slowly varying function of energy whose typical values, say, at $E = 0.01$ eV, are $6707a_0^2$ eV for $2s \rightarrow 2s$ scattering and $11\,219a_0^2$ eV for $2p \rightarrow 2p$ scattering. The $nl \rightarrow nl'$ transitions have infinite cross sections if the nl and nl' levels have opposite parity and the relativistic splitting between them is ignored [54]. The inclusion of the relativistic splitting into the Ps($2s$) $\rightarrow$ Ps($2p$) transition leads to a finite cross section which at low
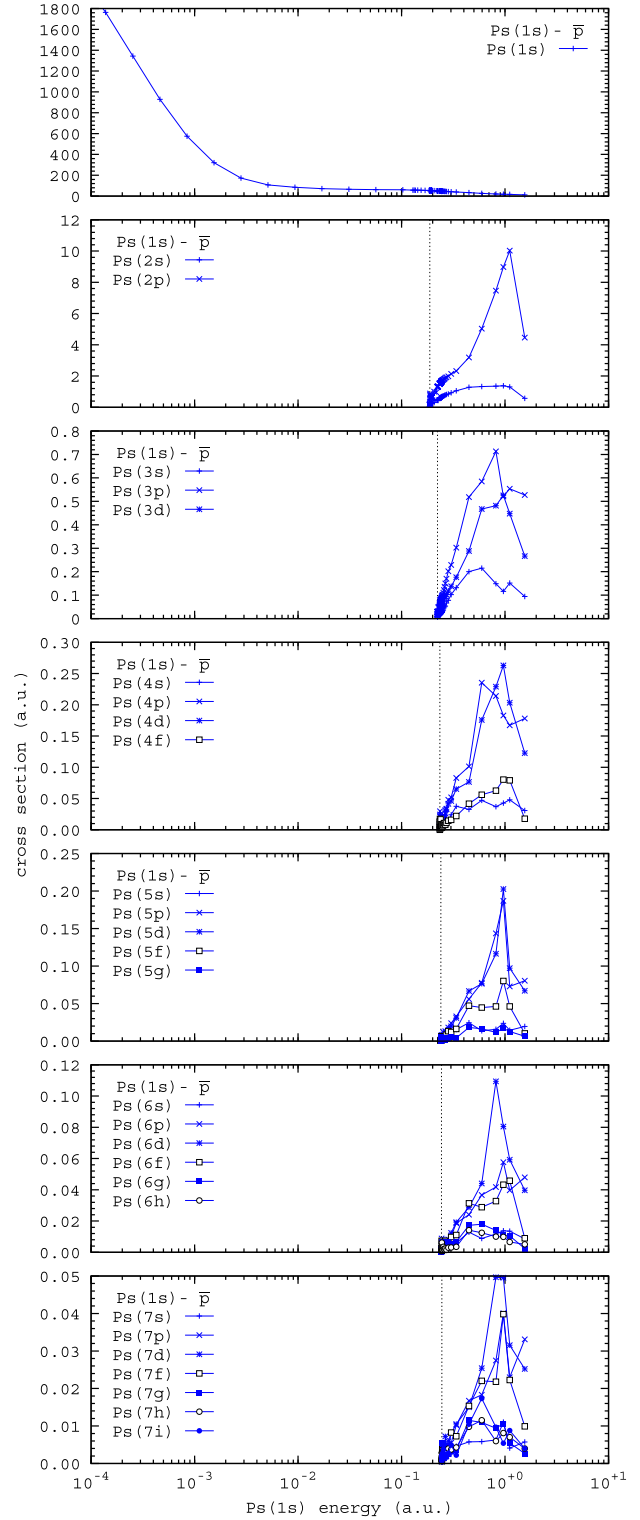

FIG. 15. CCC-calculated integrated cross sections of Ps($1s$)-Ps(n_{Ps}, l_{Ps}) transitions for Ps($1s$) $- \bar{p}$ scattering. The vertical dotted line indicates the excitation threshold.

energies behaves as $B \ln E/E$, where B is another slowly varying function of E, with $B \ln E = 55\,173a_0^2$ eV at $E = 0.01$ eV. A treatment similar to one given by Fabrikant *et al.* [52] can be applied to l-mixing collisions with a higher n_{Ps}.
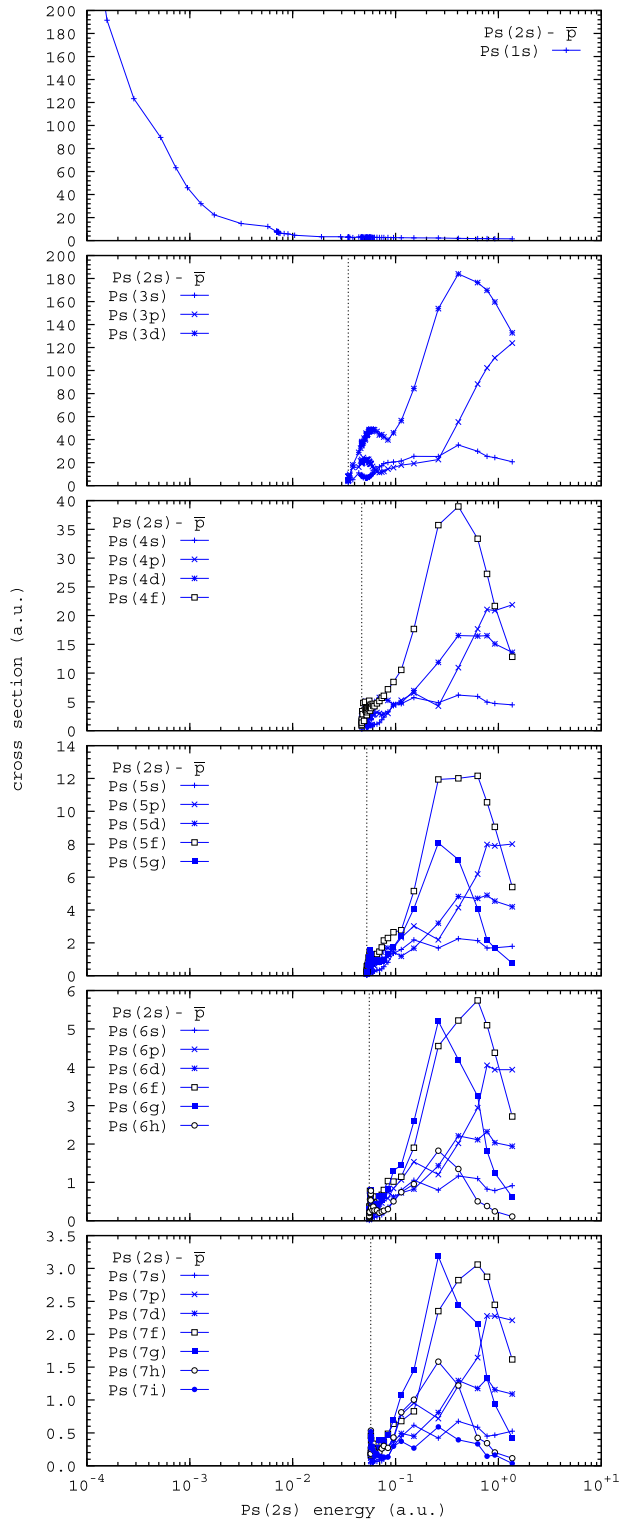
FIG. 16. CCC-calculated integrated cross sections of Ps($2s$)-Ps(n_{Ps}, l_{Ps}), $n_{Ps} \neq 2$, transitions for Ps($2s$) $- \bar{p}$ scattering.

FIG. 17. CCC-calculated integrated cross sections of Ps($2p$)-Ps(n_{Ps}, l_{Ps}), $n_{Ps} \neq 2$, transitions for Ps($2p$) $- \bar{p}$ scattering.

The Ps($1s$) data are presented in Fig. 15, where the $1s$-$1s$ cross section is obviously dominant. For the endothermic reactions [which open at ($E_{th}^{Ps} = (n_{Ps}'^2 - n_{Ps}^2)/4n_{Ps}^2 n_{Ps}'^2$)] the Ps p- and d states tend to be the most important across the n_{Ps} manifold, but overall with low probability.
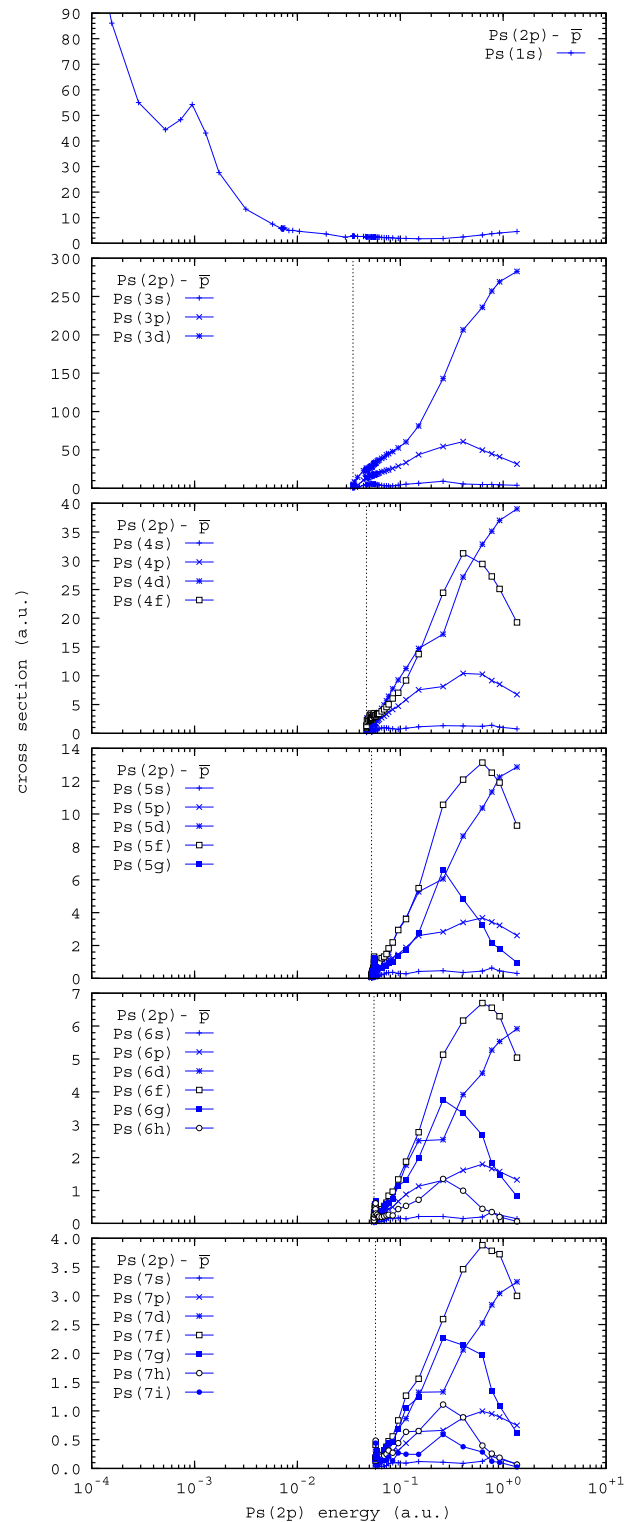
The Ps($2s$) and Ps($2p$) results are given in Figs. 16 and 17, where they can be seen to be comparable in size to the cross sections for $\overline{H}$ formation (Figs. 10 and 11) in the same Ps kinetic energy range. The exothermic $n_{Ps} = 2$-1 channel has a high cross section below the threshold for Ps excitation, but above that transfer to $n_{Ps} = 3$ states dominates, and in
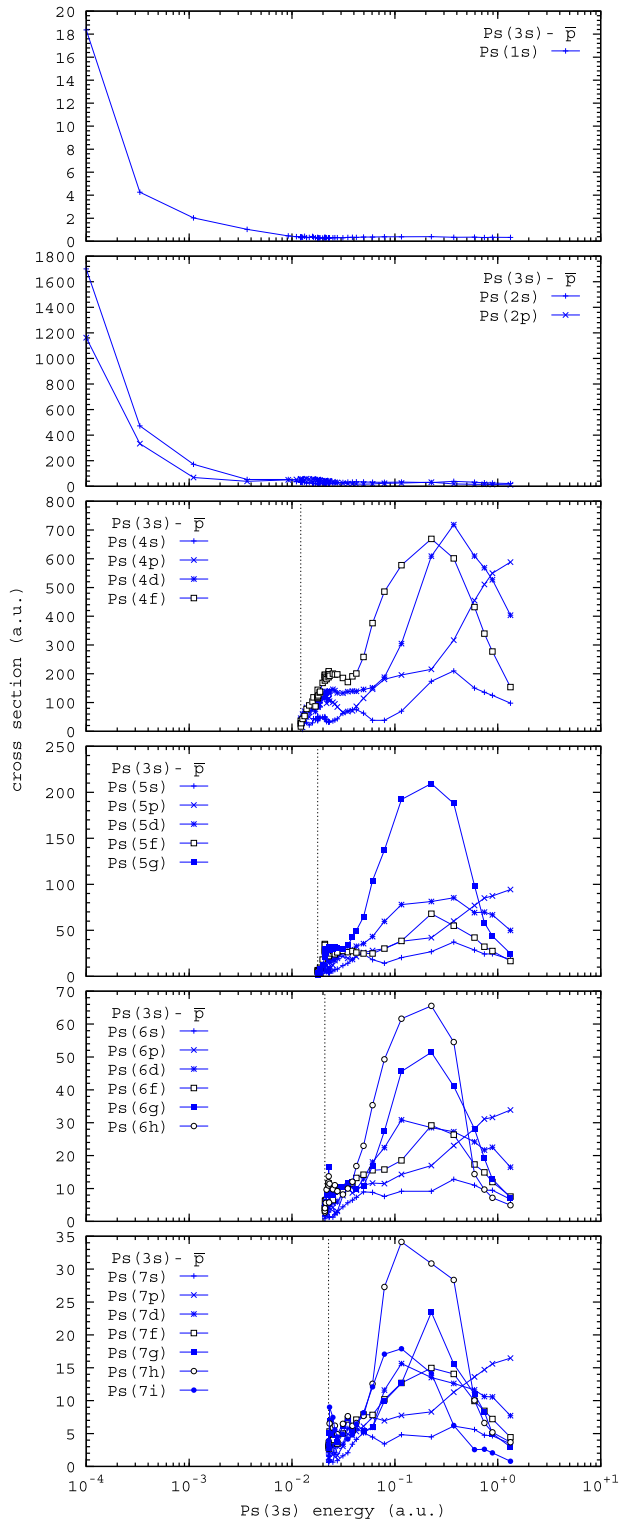
FIG. 18. CCC-calculated integrated cross sections of Ps(3*s*)-Ps(n_{Ps}, l_{Ps}), $n_{Ps} \neq 3$, transitions for Ps(3*s*) $- \bar{p}$ scattering.

FIG. 19. CCC-calculated integrated cross sections of Ps(3*p*)-Ps(n_{Ps}, l_{Ps}), $n_{Ps} \neq 3$, transitions for Ps(3*p*) $- \bar{p}$ scattering.

particular to the 3*d* state. It is notable, though, that while the cross sections for some states peak and turn over not far above threshold, others level off, or keep rising with Ps kinetic energy; this is particularly notable for the final *d* states in the 2*p* data set.
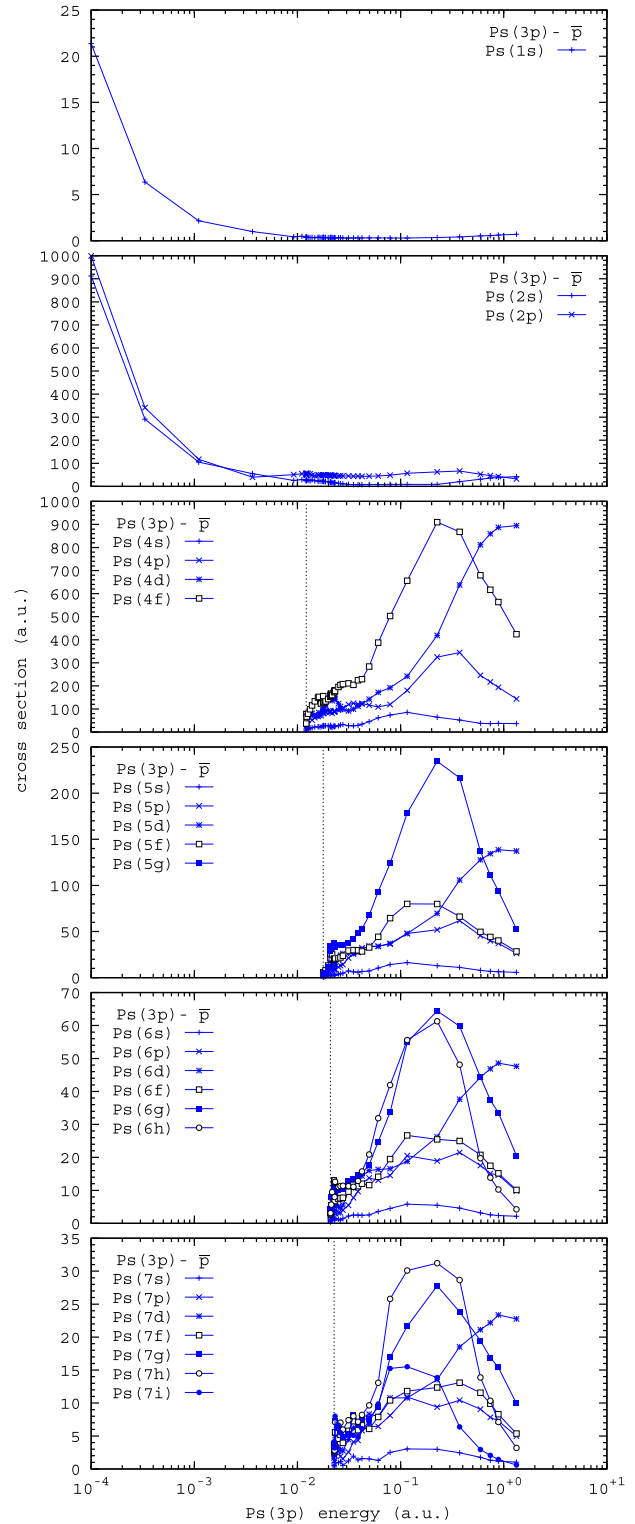
The Ps($n_{Ps} = 3$) results are presented in Figs. 18–20. As was the case with the $n_{Ps} = 2$ data, there are complex dependencies on final state. The cross sections for transfer into the respective *s* states are typically small, but there are important contributions to the overall cross section from several angular momentum states.
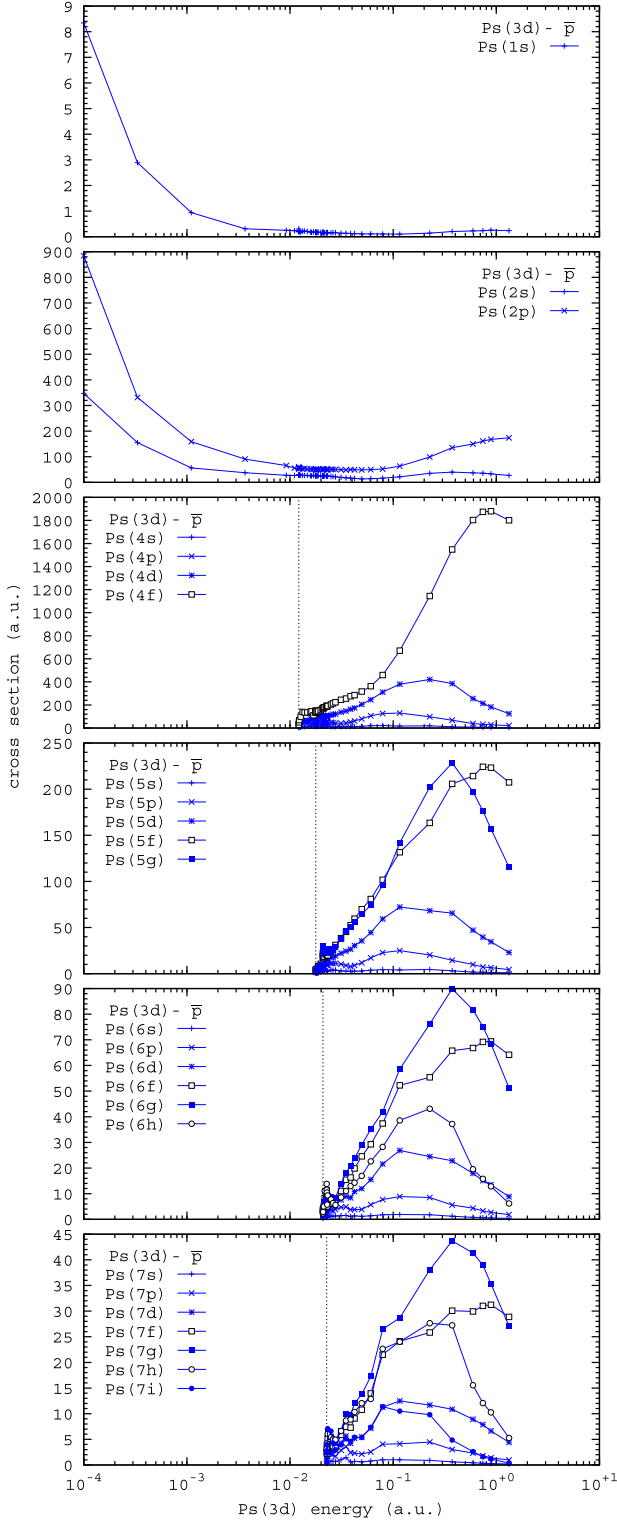
FIG. 20. CCC-calculated integrated cross sections of Ps(3*d*)-Ps(n_{Ps}, l_{Ps}), $n_{\mathrm{Ps}} \neq 3$, transitions for Ps(3*d*) − $\bar{p}$ scattering.

Taken together, the data presented herein should allow a detailed time-dependent Ps(n_{Ps}, l_{Ps}) population and its interactions with antiprotons and antihydrogen to be constructed for $\overline{\mathrm{H}}$ formation, followed, if appropriate, by in-flight spontaneous de-excitation to the ground state, to allow the most accurate predictions of $\overline{\mathrm{H}}^+$ yields to date (see, e.g., Ref. [55]).

This should enable optimization of the Ps conditions to achieve the best antihydrogen ion yield.

IV. CONCLUDING REMARKS

Generally, quantum and classical results converge well for higher n_{Ps}. However, the breakup cross sections exhibit some differences which grow with n_{Ps}, as can be seen from Figs. 2–8. The small differences in the region of the cross section maximum can be explained by the slow convergence of the CCC results with increasing orbital angular momentum l of both the $\overline{\mathrm{H}}$ and Ps states for the larger n_{Ps}. Even though we took $l \leqslant 9$, examination of the individual l contributions to breakup shows that the $l = 9$ contribution can still be large, even for the case of the Ps(7*s*) initial state. Nevertheless, due to unitarity, the CCC method is able to achieve better convergence in the total breakup cross section than in the individual l components [56]. Note that this problem is of no consequence at the lower energies, or the smaller n_{Ps}, considered.

In the breakup threshold region the CTMC results can be fit by the Wannier-Klar law, whereas the CCC results are different, probably again due to computational difficulties in calculation of very small cross sections in the near-threshold regions. This will be a focus of study elsewhere.

Due to the accuracy of the classical results for high-enough n_{Ps}, it will be reliable to estimate cross sections for even higher n_{Ps} (than those studied in the present paper) using the classical method. Moreover, it is possible to generate these cross sections from the present cross sections using the classical scaling laws as discussed above. This should keep the uncertainties associated with the scaled theoretical cross sections for $n_{\mathrm{Ps}} > 7$ sufficiently small (on the order of 10%) for practical purposes.

Here we have glossed over any possible resonances or oscillations that can be found in individual partial waves for specific transitions. The degeneracy of the energy levels for a given principal quantum number n can lead to remarkable above-threshold oscillations and below-threshold dipole-supported resonances, as has been demonstrated by Fabrikant *et al.* [52]. However, upon summation over all partial waves of total orbital angular momentum such structures become indiscernible in the total integrated cross sections presented here.

In this work we have provided the most complete and accurate state-scaled data sets (up to the Ps principal quantum number $n_{\mathrm{Ps}} = 7$) for the modeling of experiments seeking to form antihydrogen using Ps($n_{\mathrm{Ps}}l_{\mathrm{Ps}}$) − $\bar{p}$ interactions, including results for the competing reactions of Ps breakup and collision-induced state change. The Ps kinetic energy region in which $\overline{\mathrm{H}}$ formation is dominant has been clearly outlined. By detailed comparison of data from the CCC and CTMC approaches we have confirmed scaling laws, and thus provided a means to derive accurate cross section data for $n_{\mathrm{Ps}} > 7$, which will be of great value for the planning of experiments aiming to operate in this range.

[1] G. B. Andresen, M. D. Ashkezari, M. Baquero-Ruiz, W. Bertsche, P. D. Bowe, E. Butler, C. L. Cesar, S. Chapman, M. Charlton, A. Deller (ALPHA Collaboration) *et al.*, Nature (London) **468**, 673 (2010).

[2] G. Gabrielse, R. Kalra, W. S. Kolthammer, R. McConnell, P. Richerme, D. Grzonka, W. Oelert, T. Sefzick, M. Zielinski, D. W. Fitzakerley, (ATRAP Collaboration), Phys. Rev. Lett. **108**, 113002 (2012).

[3] M. Ahmadi, B. X. R. Alves, C. J. Baker, W. Bertsche, E. Butler, A. Capra, C. Carruth, C. L. Cesar, M. Charlton, S. Cohen, (ALPHA Collaboration) *et al.*, Nat. Commun. **8**, 681 (2017).

[4] M. Ahmadi, B. X. R. Alves, C. J. Baker, W. Bertsche, E. Butler, A. Capra, C. Carruth, C. L. Cesar, M. Charlton, S. Cohen, Nature (London) **548**, 66 (2017).

[5] M. Ahmadi, B. X. R. Alves, C. J. Baker, W. Bertsche, A. Capra, C. Carruth, C. L. Cesar, M. Charlton, S. Cohen, R. Collister, (ALPHA Collaboration) *et al.*, Nature (London) **557**, 71 (2018).

[6] M. Ahmadi, B. X. R. Alves, C. J. Baker, W. Bertsche, A. Capra, C. Carruth, C. L. Cesar, M. Charlton, S. Cohen, R. Collister, (ALPHA Collaboration) *et al.*, Nature (London) **561**, 211 (2018).

[7] C. J. Baker, W. Bertsche, A. Capra, C. Carruth, C. L. Cesar, M. Charlton, A. Christensen, R. Collister, A. Cridland Mathad, S. Eriksson (ALPHA Collaboration) *et al.*, Nature (London) **592**, 35 (2021).

[8] M. Charlton, S. Eriksson, and G. M. Shore, in *Antihydrogen and Fundamental Physics* (Springer, Switzerland, 2020), pp. 1–95.

[9] P. Belochitskii, T. Eriksson, and S. Maury, Nucl. Instrum. Methods Phys. Res., Sect. B **214**, 176 (2004), low Energy Antiproton Physics (LEAP'03).

[10] W. Bartmann, P. Belochitskii, H. Breuker, F. Butin, C. Carli, T. Eriksson, W. Oelert, R. Ostojic, S. Pasinelli, and G. Tranquille, Philos. Trans. R. Soc. A **376**, 20170266 (2018).

[11] W. A. Bertsche, Philos. Trans. R. Soc. A **376**, 20170265 (2018).

[12] M. Doser, C. Amsler, A. Belov, G. Bonomi, P. Bräunig, J. Bremer, R. Brusa, G. Burkhart, L. Cabaret, C. Canali (AEgIS Collaboration) *et al.*, Class. Quantum Grav. **29**, 184009 (2012).

[13] D. P. van der Werf, Int. J. Mod. Phys. Conf. Ser. **30**, 1460263 (2014).

[14] D. B. Cassidy, Euro. Phys. J. D **72**, 53 (2018).

[15] C. Amsler, M. Antonello, and A. Belov (AEgIS), Phys. Comm. **4**, 19 (2021).

[16] J. P. Merrison, H. Bluhme, J. Chevallier, B. I. Deutch, P. Hvelplund, L. V. Jørgensen, H. Knudsen, M. R. Poulsen, and M. Charlton, Phys. Rev. Lett. **78**, 2728 (1997).

[17] A. S. Kadyrov and I. Bray, Phys. Rev. A **66**, 012710 (2002).

[18] D. Krasnický, R. Caravita, C. Canali, and G. Testera, Phys. Rev. A **94**, 022714 (2016).

[19] H. B. Ambalampitiya, D. V. Fursa, A. S. Kadyrov, I. Bray, and I. I. Fabrikant, J. Phys. B: At., Mol. Opt. Phys. **53**, 155201 (2020).

[20] A. S. Kadyrov, C. M. Rawlins, A. T. Stelbovics, I. Bray, and M. Charlton, Phys. Rev. Lett. **114**, 183201 (2015).

[21] C. M. Rawlins, A. S. Kadyrov, A. T. Stelbovics, I. Bray, and M. Charlton, Phys. Rev. A **93**, 012709 (2016).

[22] M. Charlton, A. S. Kadyrov, and I. Bray, Phys. Rev. A **94**, 032701 (2016).

[23] A. S. Kadyrov, I. Bray, M. Charlton, and I. I. Fabrikant, Nat. Commun. **8**, 1544 (2017).

[24] M. Charlton, H. B. Ambalampitiya, I. I. Fabrikant, D. V. Fursa, A. S. Kadyrov, and I. Bray, Phys. Rev. A **104**, L060803 (2021).

[25] W. A. Bertsche, M. Charlton, and S. Eriksson, New J. Phys. **19**, 053020 (2017).

[26] A. S. Kadyrov and I. Bray, J. Phys. B: At. Mol. Opt. Phys. **49**, 222002 (2016).

[27] I. Bray, J. J. Bailey, D. V. Fursa, A. S. Kadyrov, and R. Utamuratov, Eur. Phys. J. D **70**, 6 (2016).

[28] A. S. Kadyrov, I. Bray, and A. T. Stelbovics, Phys. Rev. Lett. **98**, 263202 (2007).

[29] R. Abrines and I. C. Percival, Proc. Phys. Soc. **88**, 873 (1966).

[30] I. C. Percival and D. Richards, Adv. At. Mol. Phys. **11**, 1 (1976).

[31] D. Krasnicky, G. Testera, and N. Zurlo, J. Phys. B: At., Mol. Opt. Phys. **52**, 115202 (2019).

[32] H. B. Ambalampitiya, J. Stallbaumer, and I. I. Fabrikant, Phys. Rev. A **105**, 043111 (2022).

[33] S. J. Aarseth and K. Zare, Celestial Mech. **10**, 185 (1974).

[34] H. B. Ambalampitiya, Semiclassical methods in atomic and molecular physics, Ph.D. thesis, University of Nebraska-Lincoln (2021).

[35] J. W. Humberston, P. V. Reeth, M. S. T. Watts, and W. E. Meyerhof, J. Phys. B: At. Mol. Opt. Phys. **30**, 2477 (1997).

[36] G. H. Wannier, Phys. Rev. **90**, 817 (1953).

[37] H. Klar, J. Phys. B: At. Mol. Phys. **14**, 4165 (1981).

[38] L. D. Landau and E. M. Lifshitz, *Mechanics*, 3rd ed., Course of theoretical physics (Pergamon Press, Oxford, 1969) Chap. 19 and 20.

[39] D. Vrinceanu, Phys. Rev. A **72**, 022722 (2005).

[40] I. Bray, A. W. Bray, D. V. Fursa, and A. S. Kadyrov, Phys. Rev. Lett. **121**, 203401 (2018).

[41] B. I. Deutch, M. Charlton, M. H. Holzscheiter, P. Hvelplund, L. V. Jørgensen, H. Knudsen, G. Laricchia, J. P. Merrison, and M. R. Poulsen, Hyperfine Interact. **76**, 151 (1993).

[42] D. B. Cassidy, T. H. Hisakado, H. W. K. Tom, and A. P. Mills, Phys. Rev. Lett. **108**, 043401 (2012).

[43] S. Aghion, C. Amsler, A. Ariga, T. Ariga, G. Bonomi, P. Bräunig, J. Bremer, R. S. Brusa, L. Cabaret, M. Caccia (AEgIS Collaboration) *et al.*, Phys. Rev. A **94**, 012507 (2016).

[44] A. M. Alonso, S. D. Hogan, and D. B. Cassidy, Phys. Rev. A **95**, 033408 (2017).

[45] C. J. Baker *et al.*, J. Phys. B: At. Mol. Opt. Phys. **51**, 035006 (2018).

[46] P. Froelich, T. Yamashita, Y. Kino, S. Jonsell, E. Hiyama, and K. Piszczatowski, Hyperfine Interact. **240**, 46 (2019).

[47] T. Yamashita, Y. Kino, E. Hiyama, S. Jonsell, and P. Froelich, New J. Phys. **23**, 012001 (2021).

[48] P. Comini and P.-A. Hervieux, New J. Phys. **15**, 095022 (2013).

[49] P. Comini, P.-A. Hervieux, and K. Lévêque-Simon, New J. Phys. **23**, 029501 (2021).

[50] M. Gailitis and R. Damburg, Proc. Phys. Soc. (London) **82**, 192 (1963).

[51] M. Gailitis, J. Phys. B: At. Mol. Phys. **15**, 3423 (1982).

[52] I. I. Fabrikant, A. W. Bray, A. S. Kadyrov, and I. Bray, Phys. Rev. A **94**, 012701 (2016).

[53] I. I. Fabrikant, A. S. Kadyrov, I. Bray, and M. Charlton, J. Phys. B: At. Mol. Opt. Phys. **50**, 134001 (2017).

[54] M. Gailitis, J. Phys. B **11**, L279 (1978).

[55] P. Comini, P.-A. Hervieux, and F. Biraben, Hyperfine Interact. **228**, 159 (2014).

[56] I. Bray, Phys. Rev. Lett. **73**, 1088 (1994).